Ionization and Fragmentation of Methane Induced by 40 eV to 480 eV Synchrotron Radiation: From Valence to Beyond Core Electron Ionization

ARTICLE *in* THE JOURNAL OF PHYSICAL CHEMISTRY A · DECEMBER 2012

Impact Factor: 2.69 · DOI: 10.1021/jp309187d · Source: PubMed

7 AUTHORS, INCLUDING:

Vitor Luiz Bastos de Jesus
Instituto Federal de Educação, Ciência e Tecn…
56 PUBLICATIONS **736** CITATIONS
SEE PROFILE

Reinaldo Cavasso-Filho
Universidade Federal do ABC (UFABC)
48 PUBLICATIONS **267** CITATIONS
SEE PROFILE

A. C. F. Santos
Federal University of Rio de Janeiro
137 PUBLICATIONS **871** CITATIONS
SEE PROFILE

THE JOURNAL OF PHYSICAL CHEMISTRY A

Article

pubs.acs.org/JPCA

Ionization and Fragmentation of Methane Induced by 40 eV to 480 eV Synchrotron Radiation: From Valence to Beyond Core Electron Ionization

W. Wolff,[†,*] L. Sigaud,[†] E. C. Montenegro,[†] V. L. B. de Jesus,[‡] R. L Cavasso Filho,[§] S. Pilling,[⊥] and A. C. F. Santos[†]

[†]Instituto de Física, Universidade Federal do Rio de Janeiro, PO 68528, 21941-972 Rio de Janeiro, RJ, Brazil

[‡]Instituto Federal de Educação, Ciência e Tecnologia do Rio de Janeiro (IFRJ), Campus Nilópolis, R. Lucio Tavares 1045, 26530-060 Nilópolis, RJ, Brazil

[§]Universidade Federal do ABC, Rua Catequese 242, 09090-400, Santo André, SP, Brazil

[⊥]Universidade do Vale do Paraíba, UNIVAP, Av. Shishima Hifumi 2911, Campus Urbanova, 12244 000, São José dos Campos, SP, Brazil

ABSTRACT: Photoionization and fragmentation of gaseous methane induced by tunable synchrotron radiation were investigated in a wide energy range, from 40 eV up to 480 eV. We report electron-ion coincidence experiments by measuring the relative partial-ion yields and precursor-specific relative yields for individual fragment ions and for ion fragment pairs as a function of photon energy. The fragmentation patterns are discussed with emphasis on the transition behavior of the bond breaking reactions and of the hydrogen rearrangements from valence to core electron ionization. Below the C 1s threshold, a comparison between photon induced dissociation and electron impact data showed that the ionic fragments formation depends for both projectiles on the same final electronic state reached upon ionization.

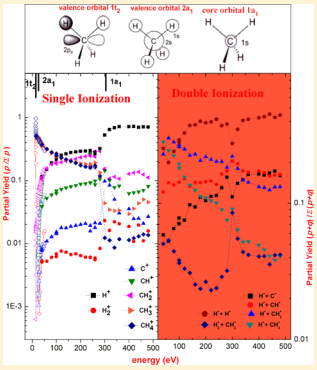

1. INTRODUCTION

Methane is detected in a variety of terrestrial and extraterrestrial environments, where ionization events are common. For planetary aeronomy, the total and relative partial-ionization cross sections and precursor-specific relative partial-ionization cross sections for fragment ions formed by irradiation are relevant in interpreting abundance and physical distributions of the molecules, which form the planetary atmospheres.[1] The fragmentation of methane induced by UV photons, soft X-rays, electron and ion impact produces reactive ionic and neutral radicals, allowing the formation of more complex molecules.

Methane is the most abundant of the minor constituents in the upper atmospheres of the outer planets: Mars, Jupiter (0.3%), Saturn (0.4%), Uranus (2%), and Neptune (1.5%).[2] As such, it is the dominant continuous photoabsorber in these atmospheres. Saturn's satellite Titan contains 1.6% methane in its atmosphere, periodically raining liquid methane onto its surface, and it has methane spewing volcanoes and methane lakes near the polar regions.[2,3] Methane has been detected in meteorites, in comets' tails,[4] and in young stars in molecular clouds.[5] Traces of methane gas are also present in the Earth's atmosphere.[6]

Methane belongs to the group of saturated molecules in which all valence electrons are involved in the formation of single bonds. It has four valence bonding molecular orbitals and there are no nonbonded lone pairs. Therefore, the molecule is generally less reactive than either electron-rich or electron-deficient species, with all occupied orbitals having relatively low energies. In the neutral ground state, the CH_4 molecule has regular tetrahedral symmetry and its electronic configuration, T_d point-group symmetry, is considered to be $(1a_1)^2(2a_1)^2(1t_2)^6\tilde{X}^1A_1$ on a single configuration basis.[7−10] Whereas the singly molecule CH_4^+ has the same ground state geometry as CH_4, the doubly charged CH_4^{2+}, with six valence electrons, is planar in its ground state, D_{4h} point-group symmetry.[11,12] The monocations and dications are generally unstable species dissociating into fragments with high kinetic energies. Thus, the dissociative processes play an important role in the selective photochemistry and as sources of other smaller cations, such as protons,[13] which can recombine or associate to other molecules or atoms.

Both valence-electron and core−electron ionization of methane have been extensively studied in the past. There have been numerous experimental and theoretical studies on the ionization of methane employing electrons[14−29] and photons[30−64] as ionizing agents. The study of photon induced

Received: September 15, 2012
Revised: December 9, 2012
Published: December 11, 2012

processes on methane started with measurements of photoabsorption cross sections[1,30−37] and photoelectron spectra using first light from nonbased synchrotron radiation, SR, such as microwave excited continuum lamp and Pt hollow line source and He I and II lamps. From the seventies onward, photoabsorption as well as photoionization cross sections were measured in the VUV and UV wavelengths using SR as excitation source. Calculations for the photoionization in the photon energy range 10−30 eV were reported in 1988.[38] Fluorescence emission and ion yields,[39] photoionization and neutral-dissociation cross sections[40] and ionization-efficiency curves for CH_n^+ (n = 2, 4)[41,42] were reported in the energy range of the valence electrons (from 10 to 30 eV). High-resolution photoabsorption cross sections,[43,44] Lyman-α and Balmer emission spectra[45] and high-resolution electron yields and electron and Auger electron spectra[46−49] following core excitation were measured in the region of the carbon 1s ionization threshold. Double ionization was studied in the energy range 35−53 eV by the photoion-photoion coincidence method[50,51] and electron energy distribution maps for the double ionization were measured by means of the TOF-PePeCo method.[52] More recently the triple ionization of methane by double Auger effect was investigated.[53]

Fragmentation yields were recorded at energies well below the C 1s threshold, 12−60 eV, and at some energy in its vicinity following selective ionization of the molecular orbitals. Ion spectra were measured in coincidence with electrons without energy discrimination by using mass spectroscopy, quadrupole or time-of-flight mass spectroscopy,[54−57] or with the photoelectron energy discriminated[58−60] and by the arrival of time correlated pairs of ions.[51] Detailed 1s core ionization studies were presented applying the Ereico technique.[61−63] In these works, energy resolved electron−ion coincidence spectra of methane and deuterated methane molecules were measured and complementary noncoincidence ion yield measurements were performed at photon energies around the 1s carbon threshold. New measurements and theoretical calculations for the photoionization of CH_4 at the carbon K-edge were performed using cold target recoil ion momentum spectroscopy (COLTRIMS) combined with complex Kohn variational calculations of the photoelectron in the molecular frame.[64]

We report here measurements from 40 eV up to 480 eV, well below and above the carbon ionization edge. The data fill the gap left by previous measurements and show in detail the transition from valence to core ionization of the dissociation processes. The purpose of the present study is 3-fold: First, to report partial yields for the single-ion production of methane induced by photons over a wide energy range, crossing the carbon atoms edge. Second, to present partial yields of ion fragment pairs, caused by the double ionization of the molecules. Third, to compare photon impact with electron impact mass spectrometry data, as they play complementary roles with each other: SR is used as a real photon source and fast inelastically scattered electrons is used as a virtual-photon source.[21]

In the next section we present the experimental setup. The data reduction and analysis are presented in section 3.1 and discussed in detail in the Appendix. The present work results of the single and multi-ionization followed by molecular fragmentation are introduced and discussed in section 3.2. In the last section, conclusions and final remarks are given.

2. EXPERIMENTAL METHODS

A soft X-ray flux of around 10^{12} photons/s was produced at the Brazilian Synchrotron Light Laboratory, LNLS, in Campinas, São Paulo, Brazil. The experiments were conducted at two different beamlines, one based on a Toroidal-Grating Monochromator, TGM beamline,[65] and the other based on a Spherical-Grating Monochromator, SGM beamline.[66] The TGM beamline delivers photons with energies varying from 12 to 280 eV, while the SGM beamline operates from 260 up to 1000 eV. The photon energy calibration was performed by measuring near-edge x-ray absorption fine structure spectroscopy (NEXAFS) of the CH_4, N_2, and O_2 molecules and comparing them with literature values.[67−70] The photons are selected with respect to their wavelength by the corresponding grating monochromator, focused with the help of phosphorescent targets and diodes and collimated by an x−y grid. Then they perpendicularly intersect the target gas sample, which is in the form of an effusive jet, and the time-of-flight mass spectrometer inside a high vacuum chamber. The positively charged ions and the ejected electrons produced by the interaction with the photon beam are accelerated by a two-stage electric field, focused by lenses and directed into opposite directions toward two microchannel plate detectors in a chevron configuration. The ions drift through a 290 mm long tube at zero electric field and are analyzed with respect to their mass-to-charge ratio, m/q. They generate up to three stop signals to a time-to-digital converter, TDC, whose start signal is triggered by one of the electrons simultaneously emitted in the collision. The same experimental chamber,[66] which includes the entrance collimation setup, the time-of-flight mass spectrometer, the injection gas jet needle setup and the light sensitive diode for recording the emergent photon beam flux, as well as the coincidence electronic setup were used in both beamline measurements. The detection angle of the TOF axis was 90 degrees with respect to the linear polarization axis of the synchrotron radiation. The base pressure of the interaction chamber was kept around 1×10^{-8}Torr and the typical sample pressure maintained in the range of $1-2 \times 10^{-6}$ Torr.

In this study, both photoelectron−photoion (PePico) and photoelectron−photoion−photoion (PePiPico) coincidence spectroscopy were used as a tool to investigate with high resolution the single ionization and multi-ionization of methane leading to its fragmentation.[71] The PePiPico measurements give information on the ion-pairs produced in the ionization event and allow the evaluation of the average kinetic energy of the charged fragments. Using a moderate extraction field of 50 V/cm, the TOF was set to collect fragment ions and electrons with kinetic energy up to 10 and 40 eV, respectively, in a solid angle of 2π.[72] Correlation between electrons and ion pairs was recorded by a fast multiple event time digitizer with 2 GHz maximum sampling rate.

3. RESULTS AND DISCUSSION

The following section is divided into two parts: the first briefly describing the detection and collection efficiency corrections applied to the measurements of the PePico and PePiPico spectra and the second presenting the results and discussing the partial yields of individual ions and of ion−ion pairs for the methane molecule.

3.1. Data Reduction of Single and Multiple Ion Arrival.

The data accumulated by the TDC is a list of ion arrival times associated with each signal of an ejected electron. The data

dx.doi.org/10.1021/jp309187d | J. Phys. Chem. A 2013, 117, 56−66

collection electronics can record events with 2 or 3 simultaneous inputs, but the majority of the events involve the arrival of just one molecular ion. The relative individual single-ion (i) yield and (ii) ratio were evaluated by summing the counts in the individual peaks and then normalizing them by (i) the total sum of all peaks' counts and (ii) by the precursor specific parent fragment ion CH_4^+ counts, respectively. In the case of double ionization, the data were normalized by total ion−ion pair counts and by the ion pair breakup channel $H^+ + CH_3^+$, which is the most energetically favorable ion-pair breakup channel.

Two-dimensional mass spectra were generated from the multiple arrivals by constructing a two-dimensional histogram of flight times of both ions. In most ion-pair breakup channels, more than two fragments, charged or neutral, are produced. In this study, we focus our interest in the information regarding the relative yields in the transition from valence to core ionization that can be derived from the recorded one- and two-dimensional spectra.

In order to evaluate the partial yield of all single-ion p and ion-pair breakup $(p + q)$ channels from the areas measured from the single-events spectra and coincidence maps, several corrections have to be made besides the correction for the detection efficiencies of the different channels. Normalization procedures and corrections were applied in order to take into account: lost fragments, random coincidences, ^{13}C isotope and contaminants in the target gas, background contribution, second harmonic contribution, mass discrimination effects: detection efficiency of the light mass H^+ ion and of singly and doubly ionized ions, contribution to ion−ion pairs: dead time losses detecting $H^+ + H^+$-pairs, and beamline performance correction. These corrections are presented in detail in the Appendix.

Several dotted lines, shown to guide the eye, were included in all figures presenting partial yields or ratios, so as to depict more easily the transition behavior of the data of the several cation species with the photon energy. In the same figures error bars indicate the uncertainties, where the uncertainties of the ions peak intensities were relatively low (∼1−6%) in comparison with all the corrections factors applied. The SGM beamline data were subjected to higher second harmonic and lost fragment contributions than the TGM beamline data and thus the applied corrections increase the uncertainties. The one-dimensional data present uncertainties varying between 6 and 18%, while two-dimensional data fluctuates between 10 and 30%, and in both distributions the higher uncertainties are related to the H_2^+ ion.

3.2. Results. *3.2.1. Time of Flight Spectra.* The dissociation products observed in a mass-calibrated time-of-flight spectrum (Figure 1a) show the undissociated molecular ion CH_4^+, fragments without hydrogen atoms due to the breakage of one or more C−H bonds (CH_n^+ where n = 0−3), hydrogen ions and molecules (H^+ and H_2^+), and the doubly charged atomic species C^{2+}. No doubly charged parent ions, CH_4^{2+}, were detected, independently of the ionization mechanism involved.

3.2.2. Single Partial Yields. Figure 1b displays the partial yields of the various fragment ions p as a function of the photon impact energy. The data shown in the figure are given also in Tables 1 and 2, included in the Appendix. The three molecular orbital energies of methane, namely, the core MO, $1a_1$ and the valence MOs, $2a_1$ and the 3-fold degenerate MOs $1t_2$,[66,67] are included in the figure.

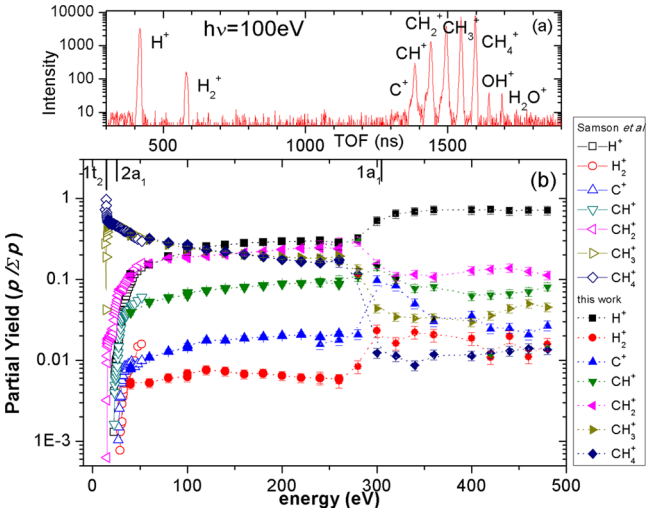

Figure 1. (a) Typical time-of-flight spectrum; (b) Partial yields of single photoionization of CH_4 as a function of the photon energy. Open symbols: ref 55. Closed symbols: this work. p denominates the ion fragment. The binding energies of the core MO $1a_1$ and the valence MOs, $2a_1$, and the 3-fold degenerate MOs, $1t_2$, are indicated by long bars.

The H^+ yield, at the lowest photon energy presented in this work, 40 eV, was normalized to the corresponding yield from ref 55 (see Appendix, section IV). At the low energy region, where overlap with the measurements of ref 55 occurs, the present measured partial yields for all other ionic fragments almost matched the previously reported values. However, some disagreement was observed for the H_2^+ ion yields.

Around 20 eV onward, the partial yields for both the nondissociative channel (CH_4^+) and the dissociative channel corresponding to the loss of one hydrogen atom (CH_3^+) decrease slowly but continuously, until a sudden sharp drop is observed at the carbon ionization 1s-edge. The drop, in the case of the CH_4^+, is far stronger than for the CH_3^+ channel. On the other hand, in the case of the loss of two to four hydrogen atoms, the partial yields increase very weakly until the C 1s threshold. The CH_2^+ yield rises monotonically up to the edge, but the CH^+ and C^+ yields present a wide peak distribution around the edge, this feature being more pronounced for the C^+ case. After the C 1s threshold, the values for all CH_n^+ yields decrease and stay approximately constant onward, leveling off at different plateau values. In contrast, the atomic and molecular hydrogen yields follow a long rise around the inner-shell ionization energy, reaching plateau values without decreasing after the edge. After the C 1s edge, the atomic hydrogen ion is by far the most abundant fragment ion produced as more bond cleavages occur.

The loss of hydrogen atoms is depicted in Figure2, where an average loss of H atoms, $\langle n_H \rangle$, defined as

$$\langle n_H \rangle = M_{CH_4} - \sum_{M_p-12}^{16} M_p \times \mathrm{PY}(M_p) / \sum_{p=12}^{16} \mathrm{PY}(M_p) \quad (1)$$

is displayed as a function of the photon energy (M_p is the fragment mass and $\mathrm{PY}(M_p)$ the partial yield of the single channel of mass M_p). In average, before the edge one to one and a half H atoms are lost, while at the edge up to 3 H atoms can be removed and after inner shell ionization two are released.

dx.doi.org/10.1021/jp309187d | J. Phys. Chem. A 2013, 117, 56−66

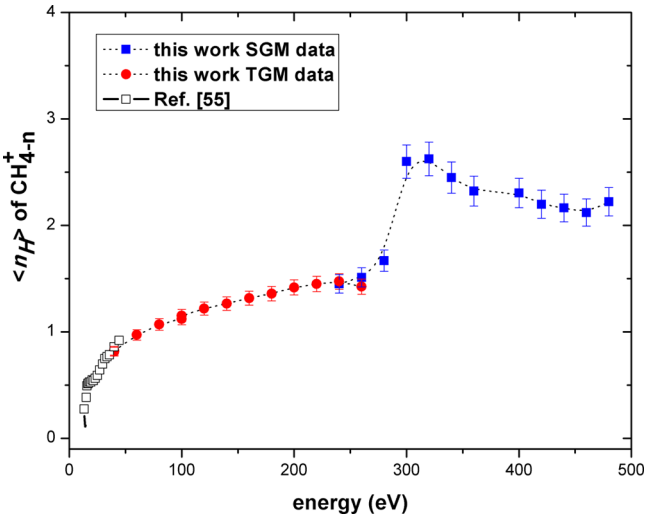

Figure 2. Average atomic hydrogen loss $\langle n_H \rangle$ as a function of the photon energy. Open squares: ref 55. Closed circles: TGM beamline measurements. Closed squares: SGM beamline measurements.

The relative abundances of the fragments with respect to the precursor parent molecular ion CH_4^+ can be related to the $(1t_2)^{-1}$, $(2a_1)^{-1}$, and $(1a_1)^{-1}$ states[73,74] assuming that the stability of the parent molecular ion is independent of the ejected electron energy.

Figure 3a shows the ratios of the measured ionic fragments relative to those of CH_4^+ as a function of the photon energy. After a sharp rise from the threshold energy up to ~50 eV, all ratios present a small growth with the increase of the photon energy until the C 1s threshold is reached, when all ratios exhibit a second sharp increase toward another set of approximate plateaus at significantly higher values.

Photons with energies well above the ionization threshold of the $(1t_2)^{-1}$ state release continuum electrons with high momentum which, in turn, are related to the characteristics of the wave function of the initial bound state near the C nucleus. Thus, the s-wave component of the hybrid orbital $1t_2$ plays a major role in this dynamical regime. As both $2a_1$ and $1a_1$ have strong components from s states, it can be expected that photoionization cross sections from all these three states depend on the photon energy E approximately as $\hat{E}(-7/2)$.[75] As a consequence, the fragmentation ratios involving different molecular orbitals of CH_4 are roughly independent of the photon energy, except at the thresholds. Comparison of the p/CH_4^+ ratios for photon energies from 50 to 250 eV (first plateau in Figure 3a) between this work and the maximum ratios observed by electron impact (Figure 3b) shows approximately the same value for CH_3^+, coming from the $(1t_2)^{-1}$ state.[21,27,28] However, the ratios for the CH_2^+, CH^+ and H^+ fragments, coming from $(2a_1)^{-1}$ (ref 21), are approximately four times larger for photon impact. For photon energies above the C 1s threshold, the large increase in all fragment yields, shown in Figure 3a, are mostly due to the multiple ionization of the parent molecule produced by the Auger cascades following the C 1s vacancy.

Figures 4a and 4b display, as a function of the transferred energy, the CH^+/CH_2^+ and H^+/CH_2^+ ratios, respectively, after a small correction due to the contribution of the $(1t_2)^{-1}$ to the production of CH_2^+ as discussed in ref 21. For comparison purposes both figures also include the data extracted from the photodissociation experiments of Samson et al.[55] as well as the electron loss measurements at 10 keV electron impact energy from ref 21.

The tendency toward a constant value for these ratios for energy transfers larger than ~30 eV is clearly discernible on the three sets of data, and verified by the present measurements. High energy transfers in both photon and electron impact are impinged directly to the swift ejected electron. Thus, the same constant ratios give evidence that the final state of the molecular ion is the same for both projectiles, as well as the fragmentation pattern.

3.2.3. Dissociative Double Photoionization. Double photoionization was studied in the low energy range of 35−52 eV by means of synchrotron radiation by Dujardin et al.[50] and at 40.8

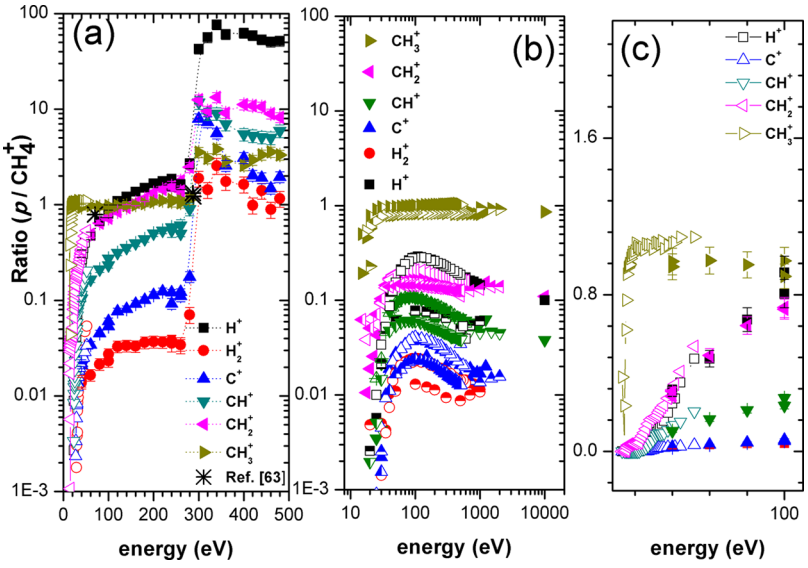

Figure 3. Abundances of all final ionic fragments p relative to the precursor parent CH_4^+ ion in log-scale as a function of the energy. (a) Photon impact data: open symbols, ref 55; large stars, ref 63; closed symbols, this work. (b) Electron impact data: closed symbols, ref 25; open symbols, ref 26; vertical half-closed symbols, ref 23; horizontal half-closed symbols, ref 18. (c) Abundances of some ionic fragments p relative to the precursor parent CH_4^+ ion in linear scale in the energy region of 10−100 eV.

dx.doi.org/10.1021/jp309187d | J. Phys. Chem. A 2013, 117, 56−66

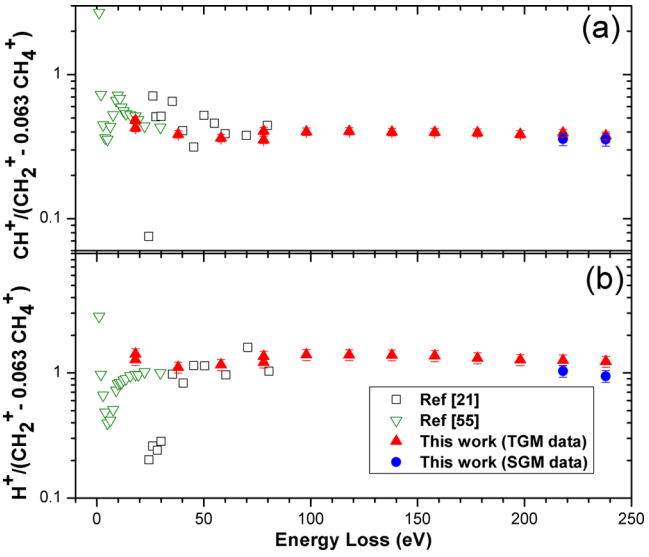

Figure 4. Fragmentation of the $(2a_1)^{-1}$ state into CH_2^+, CH^+ and H^+. (a) Ratio between CH^+ and CH_2^+ abundances, corrected for the production of CH_2^+ from the $(1t_2)^{-1}$ state (i.e., 0.063 × CH_4^+ intensity): open squares, ref 21; open down triangles, ref 55; closed up triangles, TGM beamline measurements; closed circles, SGM beamline measurements. (b) The same for H^+ and CH_2^+.

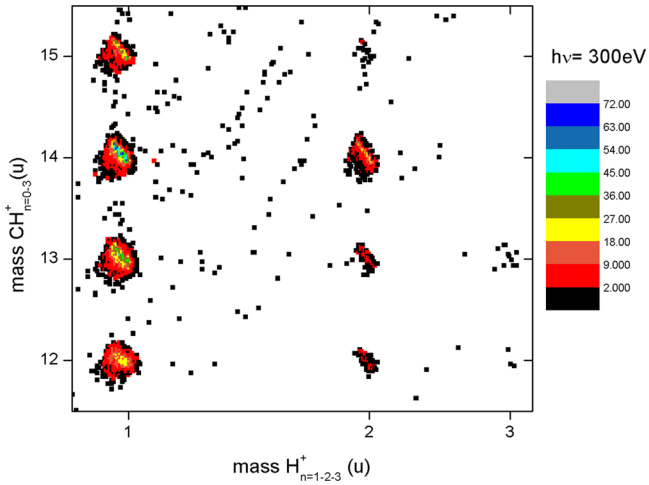

Figure 5. Coincidence map of the ion-pair breakup channels produced by 300 eV photons.

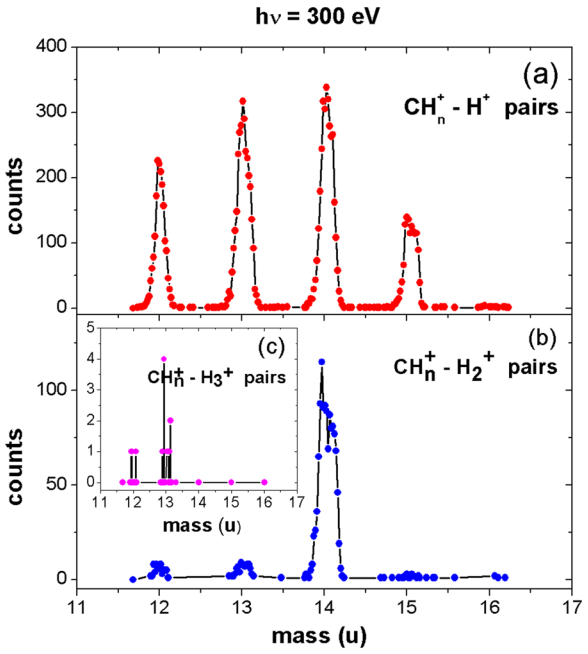

Figure 6. Mass spectra of CH_n^+ fragments (n = 0–3) in coincidence with (a) H^+; (b) H_2^+; (c) H_3^+.

eV using He II light by Fournier et al.[51] The absolute double photoionization of CH_4, reported in ref 50, passes through a maximum around 47 eV. The first observation of the decomposition of CH_4^{2+} into several singly charged fragments was done by electron impact measurements at 1 keV by McCulloh et al.[17] and later at 10 keV by Backx et al.[21]

In this work, the relative abundances of the positive ion pairs were extracted from the two-dimensional coincidence maps at photon energies from 40 to 480 eV and the dissociation channels of the unstable doubly charged CH_4^{2+} were identified. We sorted out the different cation−cation pairs corresponding to one or more dissociation channels produced by the partial or complete rupture of the C−H_n skeleton. The contribution from ion triples for all ionizing photon energies was negligible. We discriminated three pathways groups: one related to the H^+ in coincidence with H^+, H_2^+, C^+, CH^+, CH_2^+, and CH_3^+ fragments, the next associated with the molecular H_2^+ ion formation in coincidence with C^+, CH^+, and CH_2^+ and the third corresponding to the H_3^+ ion formation. Different ion pairs formed by the fragmentation of CH_4^{2+} are shown in the coincidence map of Figure 5. Parts a−c of Figure 6 display the ion-pair intensity related to the production of the three groups, $H^+ + CH_n^+$ (n = 0, 1, 2, 3), $H_2^+ + CH_n^+$ (n = 0, 1, 2), and $H_3^+ + CH_n^+$ (n = 0, 1) at an impact energy of 300 eV. In Figure 6a, it can be seen that the two-body coulomb explosion channel $H^+ + CH_3^+$ is the least pronounced breakup channel, while the three- and four-body breakup channels compete. In contrast, for the channels with H rearrangement, i.e. for $H_2^+ + CH_n^+$ and $H_3^+ + CH_n^+$ channels, the two-body ion pair configuration prevails.

3.2.4. Cation-Pairs Partial Yields. The onset of the CH_4 double ionization band is around 34 eV.[12,41,42,76−79] The lowest electronic states of CH_4^{2+} are produced by removing 2 electrons from the $1t_2$ orbital, giving rise to the multiplet of CH_4^{2+} states: $^3T_1$, $^1E_1$, $^1T_2$, and $^1A_1$. CH_4^{2+} in its $^3T_1$ state rapidly dissociates, resulting in the formation of the products $CH_3^+ + H^+$, while, at higher excitation energies, CH_4^{2+} in its $^1E_1$ state dissociates into three products: the $CH_2^+ + H^+ + H$ channel. The first channel is considered to be the most favorable dissociation pathway, both energetically and dynamically. It is energetically possible to have dissociation of CH_4^{2+} into two other cation pairs, namely $CH_2^+ + H_2^+$ and $CH^+ + H_3^+$. However, the multistep processes leading to stable hydrogen molecular ions (dissociation and association) are less likely to occur. This assumption is supported by the smaller intensity of the H_2^+ "islands" (Figures 5 and 6b) and the very weak, but still observable, H_3^+ component (Figures5 and 6c).

Some of the several possible dissociation channels are indicated in Table 4 of ref 50, where fragmentation of CH_4^{2+} into two, three, four and five products are considered. Such processes are favored in doubly charged cations due to two main reasons: (i) the threshold energy for dissociation into three fragments is below the lowest vertical double-ionization energy and (ii) the Coulomb interaction between positive charges, where the repulsive forces tend to dissociate the

dx.doi.org/10.1021/jp309187d | J. Phys. Chem. A 2013, 117, 56−66

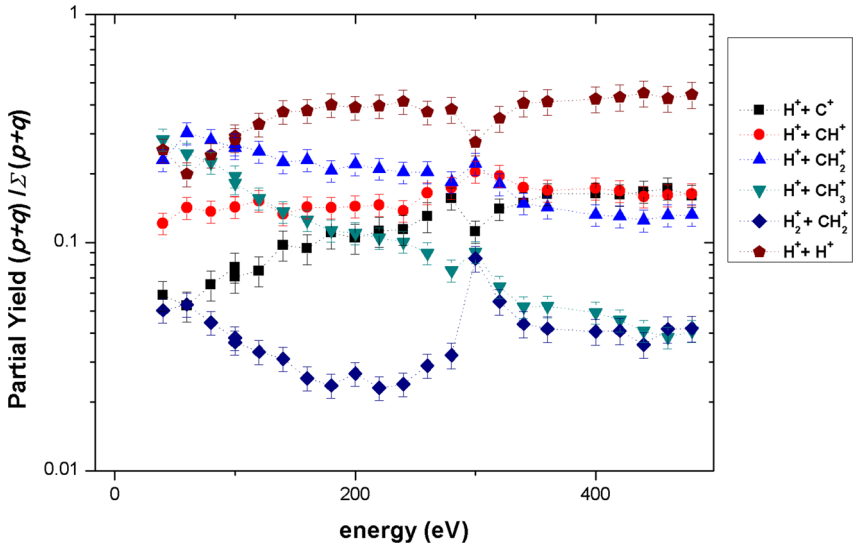

Figure 7. Partial yields of the dissociative double photoionization of CH_4 as a function of the photon energy. $(p + q)$ denominates the ion pair fragments p and q.

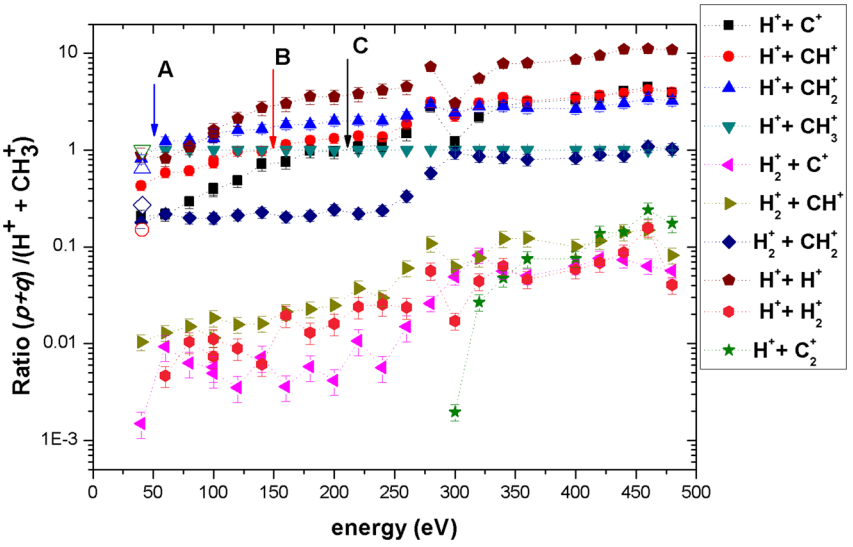

Figure 8. Abundances of all final ionic pair fragments (p +q) relative to the precursor $H^+ + CH_3^+$ ion pair as a function of the photon energy. Closed symbols: this work. Large open symbols: ref 51. The crossing points over the $H^+ + CH_3^+$channel: A, B and C of the $H^+ + CH_2^+$, $H^+ + CH^+$ and $H^+ + C^+$ channels, respectively, are indicated by arrows.

molecules into several fragments. The threshold energies for the formation of various products from CH_4^{2+}, calculated with respect to the ground state of CH_4, vary from 27.8 eV for the two fragments case, $CH_3^+ + H^+$, to 44.4 eV for the five fragments channel $C + 2H^+ + 2H$. Other possible fragmentation channels with two ionic species are: (i) $CH^+ + H^+ + H_2$, (ii) $CH^+ + H_2^+ + H$,(iii) $C^+ + H_2^+ + H_2$, (iv) $CH_2 + H^+ + H^+$, (v) $CH + H^+ + H_2^+$, (vi) $C + H_2^+ + H_2^+$, and (vii) $C + H^+ + H_3^+$. The last two channels were not observed. But after the primary dissociation of CH_4^{2+}, creating CH_n^+ fragments, the CH_n^+ can be left in a highly vibrational excited state and it is possible that the excess energy is sufficient to complete the fragmentation process.[61]

At the lowest energy measured here, 40 eV, the two channels $CH_3^+ + H^+$ and $CH_2^+ + H^+ + H$, as shown in Figure 7, compete in almost equal amounts, but as soon as the photon energy increases, the latter immediately dominates, possibly because it results from two contributions: the three fragment dissociation channel $CH_2^+ + H^+ + H$ and the secondary dissociation of the excited CH_3^+ into the pair $CH_2^+ + H$ from the two fragment dissociation channel $CH_3^+ + H^+$. The CH_3^+ ion is stable but needs only a few eV to dissociate into 2 fragments, either $CH_2^+ + H$ or $CH^+ + H_2$, or into three products $C^+ + H_2 + H$ (see Table 3 of ref 61). In the latter case the required dissociation energy is much greater and it reflects on a lower partial yield value when compared to the other channels. The most abundant expected pair during the H_2^+ formation is the two body $H_2^+ + CH_2^+$ pair,[50,51] which agrees with our observation, being by far the stronger H_2^+ component observed. The other pairs were observed, but with considerable lower abundance. The dominant ionic pair is the $H^+ + H^+$ pair, which appears due to several fragmentation channels, but in contrast to most other branching ratios, its value falls at the C 1s edge. The sudden and short drop observed in the $H^+ + H^+$ and $H^+ + C^+$ pairs only at the carbon edge can be explained by the resonant Auger spectator process, which gives preference to the production of

dx.doi.org/10.1021/jp309187d | J. Phys. Chem. A 2013, 117, 56−66

single charged fragments followed by neutral fragments.[49,80] In fact the single partial-ion yields of H^+, CH^+ and C^+ increase at the edge, as shown in Figure 1b. On the other hand, the drop in $H^+ + H^+$ pairs due to their rapid creation at the carbon edge and their loss also due to high kinetic energies could likewise explain this feature. But, the missing pairs, $H^+ + H^+$, that are lost in the "dead time region" of the data acquisition system, were added in the intensity evaluation, as described in the Appendix, section V. Around 300 eV, (C 1s edge energy), the correction factor of the missing $H^+ + H^+$ pairs was only 10% higher than the mean constant value applied to all other energies. From the distributions, shown in Figure 9c, the kinetic energies of the H^+ fragments were estimated to be up to ~20 eV. However, the spectrometer was designed to collect ionic fragments with energies up to 30 eV, meaning that almost all fragments up to this energy limit should have been collected.[72]

In order to get an idea of the stepwise indirect double ionization, the relative yields of the ion pairs relative to the precursor ion pair $H^+ + CH_3^+$ were evaluated and are shown in Figure 8. Even at the lowest measured energy value the $H^+ + CH_2^+$ ratio is greater than 1, while only around 150 eV the $H^+ + CH^+$ ratio surpasses the unity. The $H^+ + C^+$ ratio reaches unity only around 220 eV, near the C 1s edge ionization energy. The crossing points over the ion pair $H^+ + CH_3^+$ channel of the $H^+ + CH_2^+$, $H^+ + CH^+$, and $H^+ + C^+$ channels are indicated by arrows A, B, and C, respectively, in Figure 8. At the edge all former discussed ratios exhibit a sharp decline, but after it these ratios rise monotonically, reaching almost the same level. The $H^+ + H^+$ ratio is always larger than unity, but shows a decrease at the carbon edge, as does the $H^+ + C^+$ ratio. All ratios related to the H_2^+ formation were included in Figure 8 for completeness, but only the $H_2^+ + CH_2^+$ ratio proves substantial, as it almost reaches unity after the C 1s threshold. The ratios of the different products in dissociation of doubly charged methane of ref 51. measured at 40.8 eV photon energy are included in the Figure 8 and indicated by large open symbols. Some discrepancy is observed for the $H^+ + CH^+$ pair.

The comparison between the ion pairs productions with respect to $H^+ + CH_3^+$ for photons with energies between 50 and 250 eV and the same ratios measured for 10 keV electron impact energy from ref 21 shows quite similar values at variance with the large differences found in the single ionization case. This result points to a weaker influence on the role of the energy of the ejected electrons on the final molecular state of the doubly charged CH_4^{2+}. Final state correlation or shake up processes deal with energies which are significantly smaller than the excitation energies of CH_4^{2+}.

4. CONCLUSIONS

In this work 1D and 2D mass spectrometry (PePico and PePiPico time-of-flight technique) were used to measure the relative and precursor-specific yields for the formation of all ionic fragments following photoionization in the energy range of 40−480 eV. For impact energies below the carbon edge, the results revealed the selective ionization of the valence electrons and the high efficient opening of the excited electronic states of CH_4^+. Around the C 1s edge the ionization of the inner shell electrons showed fast electronic relaxation processes creating doubly ionized molecules and monocationic products in excited states. The comparison between photodissociation and electron impact data proved to be useful, allowing us to point out the influence of the energy of the ejected electrons on the final molecular state.

APPENDIX

The performance of the time-of-flight spectrometer is described in detail in ref 72. Although these experiments did not request high resolution and precise energy calibration, the 5−7 ns fwhm of the ions peaks and the 60 ns TOF difference between adjacent CH_n^+ distributions allowed an accurate peak intensity analysis of both one and two-dimensional distributions (Figures 1a and 6).

The corrections in the analysis of the data presented above are discussed here in detail. The main corrections performed were due to lost fragments, random coincidences, secondary harmonic contributions, mass/charge efficiency variation and dead time loss of the $H^+ + H^+$ pair. The detectors' efficiency difference between measurements, since they were taken a year apart, was also taken into account, as well as the contribution of the ^{13}C isotope, present in its natural abundance of 1.1%. Background contamination was very small, under 1%, in all measurements, with air being the contaminant present. Measurements of photon impact on both N_2 and O_2 were performed in order to subtract their contributions. No other contaminants, including H_2O, were significantly visible.

Tables 1 and 2 give partial yield data.

I. Lost Fragments

The lost fragments correction is needed because in some of the events where an ion pair $(p + q)$ is produced in a single collision only one of the ions is detected. The breakup channels producing one ion and the ones producing ion pairs contribute to counts in both the single-events spectra and coincidence

Table 1. Single Partial Yields ($p^+/\sum p^+$) as a Function of the Photon Energy and Beamline

energy (eV)	H^+	H_2^+	C^+	CH^+	CH_2^+	CH_3^+	CH_4^+
TGM Beamline Data							
40	0.114	0.005	0.008	0.039	0.104	0.359	0.370
40	0.115	0.005	0.008	0.039	0.114	0.349	0.370
60	0.150	0.005	0.011	0.052	0.156	0.309	0.317
80	0.190	0.006	0.013	0.059	0.181	0.269	0.282
100	0.216	0.006	0.014	0.063	0.194	0.239	0.268
100	0.229	0.007	0.015	0.069	0.185	0.244	0.251
120	0.252	0.008	0.018	0.072	0.195	0.225	0.230
140	0.265	0.007	0.018	0.077	0.204	0.213	0.217
160	0.278	0.007	0.019	0.080	0.213	0.202	0.202
180	0.285	0.007	0.019	0.083	0.220	0.195	0.190
200	0.291	0.006	0.020	0.088	0.233	0.187	0.175
220	0.293	0.006	0.021	0.089	0.241	0.183	0.166
240	0.298	0.006	0.019	0.093	0.246	0.180	0.159
260	0.282	0.006	0.021	0.086	0.240	0.192	0.173
SGM Beamline Data							
240	0.266	0.006	0.016	0.092	0.268	0.183	0.171
260	0.263	0.006	0.018	0.099	0.289	0.170	0.162
280	0.320	0.008	0.021	0.107	0.292	0.134	0.118
300	0.526	0.023	0.097	0.144	0.154	0.044	0.012
320	0.643	0.016	0.084	0.101	0.108	0.034	0.011
340	0.686	0.022	0.050	0.078	0.115	0.033	0.009
360	0.715	0.021	0.030	0.082	0.107	0.034	0.012
400	0.715	0.019	0.035	0.062	0.127	0.029	0.011
420	0.720	0.011	0.025	0.064	0.132	0.036	0.012
440	0.696	0.020	0.025	0.066	0.137	0.043	0.013
460	0.709	0.011	0.021	0.070	0.125	0.050	0.014
480	0.706	0.016	0.027	0.081	0.112	0.045	0.014

dx.doi.org/10.1021/jp309187d | J. Phys. Chem. A 2013, 117, 56−66

Table 2. Some Pairs−Partial Yields ($[p^+ - q^+]/\sum[p^+ - q^+]$) as a Function of the Photon Energy and Beamline

energy	H^+-C^+	H^+-CH^+	$H^+-CH_2^+$	$H^+-CH_3^+$	$H_2^+-CH_2^+$	H^+-H^+
TGM Beamline Data						
40	0.059	0.121	0.230	0.283	0.050	0.254
60	0.053	0.142	0.302	0.244	0.053	0.199
80	0.065	0.137	0.282	0.224	0.044	0.241
100	0.078	0.143	0.260	0.195	0.038	0.282
100	0.071	0.143	0.269	0.182	0.036	0.293
120	0.075	0.152	0.250	0.156	0.033	0.329
140	0.097	0.133	0.225	0.136	0.031	0.373
160	0.094	0.143	0.229	0.125	0.025	0.378
180	0.110	0.142	0.206	0.113	0.024	0.401
200	0.105	0.144	0.220	0.110	0.027	0.390
220	0.112	0.146	0.210	0.104	0.023	0.396
240	0.114	0.138	0.203	0.101	0.024	0.415
260	0.130	0.164	0.203	0.090	0.029	0.372
SGM Beamline Data						
280	0.156	0.173	0.184	0.075	0.032	0.382
300	0.112	0.204	0.222	0.091	0.085	0.275
320	0.140	0.196	0.180	0.064	0.055	0.350
340	0.149	0.174	0.148	0.052	0.044	0.407
360	0.163	0.169	0.143	0.052	0.042	0.414
400	0.164	0.173	0.132	0.049	0.041	0.425
420	0.161	0.168	0.130	0.046	0.041	0.433
440	0.167	0.159	0.125	0.041	0.036	0.451
460	0.172	0.161	0.131	0.038	0.042	0.427
480	0.160	0.163	0.132	0.041	0.042	0.445
280	0.156	0.173	0.184	0.075	0.032	0.382
300	0.112	0.204	0.222	0.091	0.085	0.275
320	0.140	0.196	0.180	0.064	0.055	0.350

maps. In order to obtain the true number of events in each channel p the following equation has to be applied:

$$S^m(p) = \epsilon_{ele1}\epsilon_{ion}S^t(p) + \sum_q \epsilon_{ele2}\epsilon_{ion}(1 - \epsilon_{ion})C^t(p + q) \quad (2)$$

where $S^m(p)$ and $S^t(p)$ are the measured and true number of the p single channel S events, respectively, $C^t(p + q)$ is the true number of $(p + q)$ ion-pair coincident C events, and ϵ_{ion} $(1 - \epsilon_{ion})$ is the probability of detecting one fragment out of two. The ϵ factors ϵ_{ele1} and ϵ_{ele2} are the efficiencies of detecting one and two electrons, respectively. The second term arise because a singly charged ion formed by dissociative multiple ionization may be detected while its correlated partner is missed, due to the ion detection efficiency or due to the dead time of the discrimination circuitry, meaning that no pairs are recorded if the second pair arrives before a certain time of the first ion.

The efficiency for detecting a single ion, ϵ_{ion}, is equal to 0.25, while for the detection of both fragments in coincidence the efficiency, $\epsilon_{p,q}$, is equal to $\mu_{p,q}$ $(\epsilon_{ion})^2$, where $\mu_{p,q}$ is the ion-pair extraction probability, which depends on the kinetic energy released in the dissociation. The ion-pair extraction probability is approximately equal to unity for ions with kinetic energy up to 30 eV because all ionic fragments released in the dissociation of CH_4 for all breakup channels are collected. Simulations were performed using the particle track software SIMION.[72] The relative detection efficiency for the ion fragments of masses 12 to 16 was considered the same[81] and it was checked by measuring the branching ratio between the light O^+ and N^+ ions issued from ionization of an induced air contamination. The ratio of the electron efficiencies, $\epsilon_{ele1}/\epsilon_{ele2}$, is equal to 1/1.4 and was determined by photo-ionization experiments with argon as target.

A similar equation describes the measured number of $(p + q)$ ion-pairs coincidences C^m:

$$C^m(p + q) = (\epsilon_{ion})^2\epsilon_{ele2}C^t(p + q) \quad (3)$$

Triple coincidences from the fragmentation of the CH_4^{3+} molecular ion are not included in the correction as they were not measurable at this counting rate. The single-ion rates are reduced the most for the H^+ fragment and for channels where many hydrogen fragments have been produced (such as H^+ + C^+ and H^+ + CH^+). On the other hand, the main single-ion channels, $CH_4^+$and CH_3^+, are not significantly affected by the lost fragment correction. The ion-pair rates are not affected by

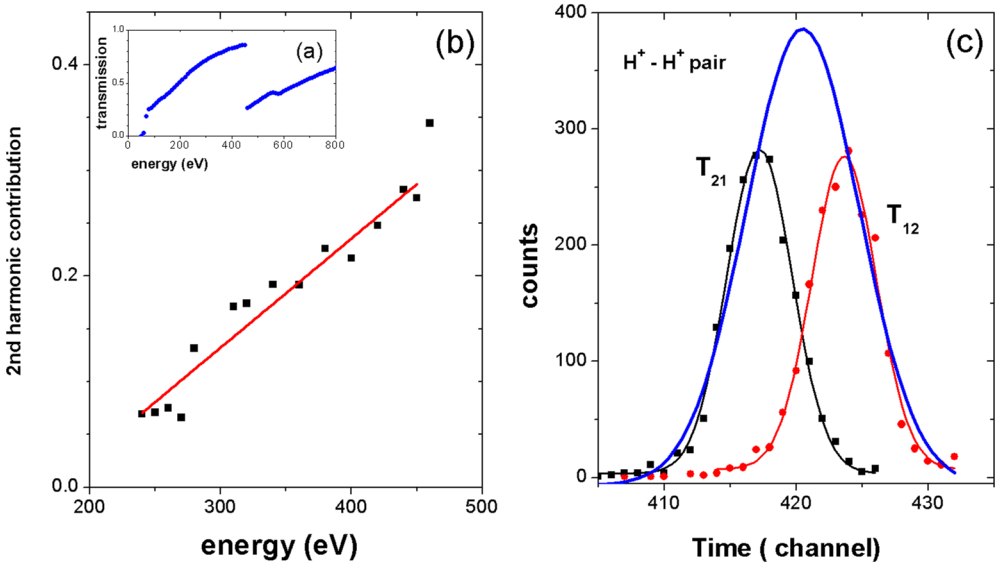

Figure 9. Data correction factors: (a) Transmission of the tungsten filter in % (ref 85); (b) second harmonic contribution in %; (c) H^+ + H^+ pair correction method.

dx.doi.org/10.1021/jp309187d | J. Phys. Chem. A 2013, 117, 56−66

this correction due to a very low random coincidence rate. The lost fragment correction contributes mostly to the C^{2+} fragments in the single-ion spectrum, as the fragmentation of a CH_4^{2+} into doubly charged carbon and four neutral hydrogen atoms is very unlikely.

II. Random Coincidences

The two dimensional spectra can contain contributions from random coincidences, where two ions which did not originate from the same dissociation event are detected simultaneously. It is caused by two collisions occurring within the same coincidence time interval selected by the multi-hit TDC module. The measured number of random coincidence counts $C^m(p + q)$ can be assessed and subtracted by an autocorrelation function of a known false island in the pairs coincidence map.

$$C^m(p + q) = R \times S^m(p) \times S^m(q) \quad (4)$$

where $S^m(p)$ and $S^m(q)$ are the measured number of counts of the single channels p and q, and R is the random coincidence coefficient. This coefficient was determined directly from the data by using the coincidence channel $H_2^+ + CH_3^+$ (Figure 5) which is purely random. The coefficient depends strongly on the counting rate, and it was completely minimized experimentally by operating at appropriate counting rates.

III. Second Harmonic Contribution

Vacuum ultraviolet beamlines based on grating monochromators have the intrinsic problem of high-order harmonics contamination,[82−84] in particular second order harmonics. By letting the light beam pass through attenuators, like thin metallic foils or gas filters with defined thickness, photons with energies higher than the attenuators ionization threshold are absorbed. In the case of the SGM line a thin tungsten foil of 1000 Å was inserted in order to minimize the second order harmonics contamination. The use of such filters is very important, since a very small portion of high-energy photons can mask the fragments generated by the first order harmonics. Figure 9a displays the transmission of the Ti-filter as a function of the photon energy.[85] Using this filter, we have performed experiments for measuring the ionization and dissociation of the diatomic molecules O_2 and N_2. By comparing the measured data with the cross section values available in the literature[86,87] a precise determination of the fraction of the second order contamination was established. Singly ionized N_2^+ and N^+, as well as O_2^+ and O^+, were measured at several energies and their double value. A degree of second order harmonic contribution was always observed. All fragments generated by the higher order harmonics had to be excluded. Figure 9b shows the percentage contamination from second harmonic energies detected using this technique and displays the fitted linear curve used to correct the SGM measurements. This procedure confirms that care must be taken when analyzing the photochemistry and dissociation dynamics with experiments in a vacuum ultraviolet beamline without the use of harmonics attenuation and diagnosis scheme. In other experiments, even if the problem of the harmonics contamination is recognized and the filter is used, the contribution to the partial yields resulting from higher order harmonics needs verification, even if the proportion of such ions can be considered of little importance.

IV. Mass Discrimination Effects: H^+, Singly and Higher Charged Ions Efficiency

When extracting quantitative data from the mass spectra it is essential to confirm that no mass discrimination effects exist. Any mass or charge-state dependent discrimination in the experiment considerably affects the relative abundances of fragment ions in the TOF mass spectra. In order to assure the detection of all ions with nearly constant efficiency we accelerate the ions setting the front channel plate voltage to 4.7 kV, 300 V higher than the drift tube voltage. When comparing our H^+ yield to the values already available in the literature for the molecules under study, we found out that our H^+ yield presented a lower efficiency than the reference data.[25] This discrepancy was corrected by introducing a multiplicative factor of 1.5. No other single charge state suffered from this deficiency.

The relative intensity of higher charged ions following radiation or particle impact ionization of targets depends on the background and target pressure, the energy with which the ions hit the MCP detector and the setting of the constant fraction discriminator used in the data collection system. The present analyzer works with the start signal generated by the electron. In double and triple ionization mechanisms two or three outgoing electrons, respectively, are available for collection. As more electrons are available as possible start signals, the probability of a coincidence event to be processed is higher. We investigated the performance of the experimental setup by measuring the relative intensities of the Ar^{2+} to Ar^+ ions and compared to the data available in the literature.[88,89] A correcting factor of 1.45 for the doubly charged ions was included in the data analysis.

V. Contribution of $H^+ + H^+$ Pairs

In addition to the corrections to the PePiPiCo spectra mentioned above, the dead time loss of $H^+ + H^+$ pairs needs to be considered. The TDC processing time (1 ns) is not fast enough to allow the simultaneous collection of all the produced $H^+ + H^+$ pairs. When quantifying the yields of this reaction contributing to the pairs spectra, the missing pairs that are lost in the "dead time region" are estimated by extrapolating the central dip or topped peaks back to $t_1 = t_2$. Considering only the positive slope of one distribution and the negative slope of the other and applying a Gaussian fit, a total net area can be attributed to the total count of $H^+ + H^+$ pair. The ratio between the total area and the summed area corresponds to the $H^+ + H^+$ correction factor. Figure 9c displays the projection of each H^+ ion's arrival time. This correction factor was obtained for each energy and fluctuates around a mean constant value of 2.4 ± 0.2.

AUTHOR INFORMATION

Corresponding Author

*E-mail: wania@if.ufrj.br.

Notes

The authors declare no competing financial interest.

ACKNOWLEDGMENTS

The authors gratefully acknowledge the support of CNPq, FAPERJ, and LNLS for this work.

REFERENCES

(1) Mount, G. H.; Warden, E. S.; Moos, H. W. *Astrophys. J.* **1977**, *214*, L47−L49.

(2) Hébrard, E.; Dobrijevic, M.; Bénilan, Y.; Raulin, F. *J. Photochem. Photobiol. C* **2006**, *7*, 211−230 and references therin..

(3) Zahnle, K.; Freedmann, R. S.; Catling, D. C. *Icarus* **2011**, *212*, 493−503.

(4) Mumma, M. J.; Disanti, M. A.; dello Russo, N.; Fomenkova, M.; Magee-Sauer, K.; Kaminski, C. D.; Xie, D. X. *Science* **1996**, *272*, 1310−1314.
(5) Lacy, J. H.; Carr, J. S.; Evans, N. J.; Baas, F.; Achtermann, J. M.; Arens, J. F. *Astrophys. J.* **1991**, *376*, 556−560.
(6) Bush, Y. A.; Schmeltekopf, A. L.; Fehsenfeld, F. C.; Albritton, D. L.; McAfee, J. R.; Goldan, P. D.; Ferguson, E. E. *Geophys. Res. Lett.* **1978**, *5*, 1027−1029.
(7) Nesbet, R. K. *J. Chem. Phys.* **1960**, *32*, 1114−1122.
(8) Slater, J. C. *Quantum Theory of Molecules and Solids*; McGraw-Hill: New York, 1963; Vol. *1*.
(9) Bieri, G.; Asbrink, L. J. *Electron Spectrosc. Relat. Phenom.* **1980**, *20*, 149−167.
(10) Herzberg, G. *Molecular Spectra and Molecular Structure*; Van Nostrand: New York, 1966, Vol. *3*, pp 583−609.
(11) Ast, T.; Porter, C. J.; Proctor, C. J.; Beynon, J. H. *Chem. Phys. Lett.* **1981**, *78*, 439−441.
(12) Siegbahn, P. E. M. *Chem. Phys.* **1982**, *66*, 443−452.
(13) Locht, R.; Olivier, J. L.; Momigny. *J. Chem. Phys.* **1979**, *43*, 425−432.
(14) Smith, L. G. *Phys. Rev.* **1937**, *51*, 263−275.
(15) Wexler, S. *J. Chem. Phys.* **1964**, *41*, 2781−2790.
(16) Fuchs, R.; Taubert, R. *Z. Naturforsch. Teil A* **1964**, *19*, 494−497.
(17) McCulloh, K. E.; Sharp, T. E.; Rosenstock, H. M. *J. Chem. Phys.* **1965**, *42*, 3501−3509.
(18) Adamczyk, B.; Boerboom, A. J. H.; Schram, B. L.; Kistemaker, J. *J. Chem. Phys.* **1966**, *44*, 4640−4642.
(19) Appell, J.; Kubach, C. *Chem. Phys. Lett.* **1971**, *11*, 486−490.
(20) Backx, C.; Wright, G. R.; Tol, R. R.; Van der Wiel, M. J. *J. Phys. B: At. Mol. Phys* **1975**, *8*, 3007−3019.
(21) Backx, C.; Van der Wiel, M. J. *J. Phys. B: At. Mol. Phys.* **1975**, *8*, 3020−3033.
(22) Chatman, H.; Hill, D.; Robertson, R.; Gallagher, A. *J. Chem. Phys.* **1984**, *81*, 1770−1777.
(23) Orient, O. J.; Srivastava, S. K. *J. Phys. B: At. Mol. Opt. Phys.* **1987**, *20*, 3923−3936.
(24) Nishimura, H.; Tawara, H. *J. Phys. B: At. Mol. Opt. Phys.* **1994**, *27*, 2063−2074.
(25) Straub, H. C.; Lin, D.; Lindsay, B. G.; Smith, K. A.; Stebbings, R. F. *J. Chem. Phys.* **1997**, *106*, 4430−4435.
(26) Tian, C.; Vidal, C. R. *J. Phys. B: Atom. Mol. Opt. Phys.* **1998**, *31*, 895−909.
(27) Wang, P.; Vidal, C. *Chem. Phys.* **2002**, *280*, 309−329.
(28) Luna, H.; Cavalcanti, E. G.; Nickles, J.; Sigaud, G. M.; Montenegro, E. C. *J. Phys. B: At. Mol. Opt. Phys.* **2003**, *36*, 4717−4729.
(29) Fainelli, E.; Maracci, F.; Avaldi, L. *J. Electron Spectrosc. Relat. Phenom.* **2002**, *123*, 277−286.
(30) Watanabe, K.; Zelikoff, M.; Inn, E. C. Y. *Air Force Cambridge Res. Center Tech. Rep.* **1953**, 53−23.
(31) Thomson, B. A.; Harteck, P.; Reeves, R. R., Jr. *Geophys. Res.* **1963**, *68*, 6431−6436.
(32) Hudson, R D. *Rev. Geophys. Space Phys.* **1971**, *9*, 305−306.
(33) Bennet, S. W.; Tellinghuisen, J. B.; Phillips, L. F. *J. Chem. Phys.* **1971**, *75*, 719−721.
(34) Starr, W. L.; Loewenstein, M. *J. Geophys. Res.* **1972**, *77*, 4790−4796.
(35) Person, J. C.; Nicole, P. P. *Argonne Nat. Lab. Rep.*: **1974**, ANL-8060.
(36) Lee, L. C.; Phillips, E.; Judge, D. L. *J. Chem. Phys.* **1977**, *67*, 1237−1246.
(37) Potts, A. W.; Price, W. C. *Proc. R. Soc. London, Ser. A* **1972**, *326*, 181−197.
(38) Cacelli, I.; Carravetta, V.; Moccia, R.; Rizzo, A. *J. Phys. Chem.* **1988**, *92*, 979−982.
(39) Sorensen, S. L.; Karawajczyk, A.; Strömholm, C.; Kirm, M. *Chem. Phys. Lett.* **1995**, *232*, 554−560.
(40) Kameta, K.; Kouchi, N.; Ukai, M.; Hatano, Y. *J. Electron Spectrosc. Relat. Phenom.* **2002**, *123*, 225−238.
(41) Dibeler, V. H.; Krauss, M.; Reese, R. M.; Harllee, F. N. *J. Chem. Phys.* **1965**, *42*, 3791−3796.
(42) Chupka, W. A. *J. Chem. Phys.* **1968**, *48*, 2337−2341.
(43) Schirmer, J.; Trofimov, A. B.; Randall, K. J.; Feldhaus, J.; Bradshaw, A. M.; Ma, Y..; Chen, C. T.; Sette, F. *Phys. Rev A* **1993**, *47*, 1136−1147.
(44) De Simone, M.; Coreno, M.; Alagia, M.; Richter, R.; Prince, K. C. *J. Phys. B: At. Mol. Opt. Phys.* **2002**, *35*, 61−75.
(45) Jakubowska, K.; Vall-llosera, G.; Kivimäki, A.; Coreno, M.; Melero Garcia, E.; Stankiewicz, M.; Rachlew, E. *J. Phys. B: At. Mol. Opt. Phys.* **2007**, *40*, 1489−1500.
(46) Ueda, K.; Okunishi, M.; Chiba, H.; Shimizu, Y.; Ohmori, K.; Sato, Y.; Shigemasa, E.; Kosugi, N. *Chem. Phys. Lett.* **1995**, *236*, 311−317.
(47) Tronc, M.; King, G. C.; Read, F. H. *J. Phys. B: At. Molec. Phys.* **1979**, *12*, 137−157.
(48) Kivimäki, A.; Neeb, M.; Kempgens, B.; Köppe, H. M.; Bradshaw, A. M. *J. Phys. B: At. Mol. Opt. Phys.* **1996**, *29*, 2701−2709.
(49) Kukk, E.; Prümper, G.; Sankari, R.; Hoshino, M.; Makochekanwa, C.; Kitajima, M.; Tanaka, H.; Yoshida, H.; Tamenori, Y.; Rachlew, E.; et al. *J. Phys. B: At. Mol. Opt. Phys.* **2007**, *40*, 3677−3692.
(50) Dujardin, G.; Winkoun, D.; Leach, S. *Phys. Rev. A* **1985**, *31*, 3027−3038.
(51) Fournier, P. G.; Fournier, J.; Salama, F.; Richardson, P. J.; Eland, J. H. D. *J. Chem. Phys.* **1985**, *83*, 241−245.
(52) Eland, J. H. D. *Chem. Phys.* **2006**, *323*, 391−396.
(53) Eland, J. H. D.; Linusson, P.; Hedin, L.; Andersson, E.; Rubensson, J. E.; Feifel, R. *Chem. Phys. Lett.* **2010**, *485*, 21−25.
(54) Kronebusch, P. L.; Berkowitz, J. *Int. J. Mass Spectrom. Ion Processes.* **1976**, *22*, 283−306.
(55) Samson, J. A.R.; Haddad, G. N.; Masuoka, T.; Pareek, P. N.; Kilcoyne, D. A. L. *J. Chem. Phys.* **1989**, *90*, 6925−6932.
(56) Field, T. A.; Eland, J. H. D. *J. Electron Spectrosc. Relat. Phenom.* **1995**, *73*, 209−216.
(57) Latimer, C. J.; Mackie, R A.; Sands, A. M.; Kouchi, N.; Dunn, K. F. *J. Phys .B: At. Mol. Opt. Phys.* **1999**, *32*, 2667−2676.
(58) Stockbauer, R. *J. Chem. Phys.* **1973**, *58*, 3800−3815.
(59) Dutuit, O.; Aït-Kaci, M.; Lamaire, J.; Richard-Viard, M. *Phys. Scr. T* **1990**, *31*, 223−226.
(60) Furuya, K.; Kimura, K.; Sakai, Y.; Takayanagi, T.; Yonekura, N. *J. Chem. Phys.* **1994**, *101*, 2720−2728.
(61) Kukk, E.; Rius i Riu, J.; Stankiewicz, M.; Hatherly, P. A.; Erman, P.; Rachlew, E.; Winiarczyk, P.; Huttula, M.; Aksela, S. *Phys. Rev. A* **2002**, *66*, 012704−1−10.
(62) Stankiewicz, M.; Winiarczyk, P.; Rius i Riu, J.; Alvarez, J.; Erman, P.; Karawajczyk, A.; Rachlew, E.; Kukk, E.; Huttula, M.; Hartherly, P. *Surf. Rev. Lett.* **2002**, *9*, 117−123.
(63) Rius i Riu, J.; Melero Garcia, E.; Alvarez Ruiz, J.; Erman, P.; Hatherly, P.; Rachlew, E.; Stankiewicz, M.; Winiarczyk, P. *Phys. Rev. A* **2003**, *68*, 022715−1−6.
(64) Williams, J. B.; Trevisan, C. S.; Schöffler, M. S.; Jahnke, T.; Bocharova, I.; Kim, H.; Ulrich, B.; Wallauer, R.; Sturm, F.; Rescigno, T. N.; Belkacem, A.; et al. *J. Phys. B: At. Mol. Opt. Phys.* **2012**, *45*, 194003-1−194003-10.
(65) Cavasso Filho, R. L.; Homem, M. G. P.; Fonseca, P. T.; Naves de Brito, A. *Rev. Sci. Instrum.* **2007**, *78*, 115104−1−9.
(66) Fonseca, P. T.; Pacheco, J. G.; d'A Samogin, E.; de Castro, A. R. B. *Rev. Sci. Instrum.* **1992**, *63*, 1256−1259.
(67) Stöhr, J., *NEXAFS Spectroscopy*; Springer Series in Surface Sciences: Berlin, 2003; Vol. *25*.
(68) Asmuruf, F. A.; Besley, N. A. *Chem. Phys. Lett.* **2008**, *463*, 267−271.
(69) Schöll, A.; Zou, Y.; Schmidt, Th.; Fink, R.; Umbach, E. *J. Electron Spectrosc. Relat. Phenom.* **2003**, *129*, 1−8.
(70) Ma, Y.; Chen, C. T.; Meigs, G.; Randall, K.; Sette, F. *Phys. Rev. A* **1991**, *44*, 1848−1858.
(71) Pilling, S.; Boechat-Roberty, H. M.; Santos, A. C. F.; de Souza, G. G. B. *J. Electron Spectrosc. Relat. Phenom.* **2007**, *155*, 70−76.

(72) Burmeister, F.; Coutinho, L. H.; Marinho, R. R. T.; Homem, M. G. P.; de Morais, M. A. A.; Mocellin, A.; Björneholm, O.; Sorensen, S. L.; Fonseca, P. T.; Lindgren.; et al. *J. Electron Spectrosc. Relat. Phenom.* **2010**, *180*, 6−13.
(73) Van Dishoeck, E. F.; Van der Hart, W. J.; Van Hemert, M. *Chem. Phys.* **1980**, *50*, 45−62.
(74) Wang, F. *J. Mol. Struct.: Theochem* **2004**, *678*, 105−111.
(75) Heitler, W. *Quantum Theory of Radiation*; Oxford University Press: London, 1954 p 207.
(76) Herzberg, G. *Electronic Spectra and Electronic Structure*; Van Nostrand: New York, 1966.
(77) Darwent, B. D. Bond dissociation energies in simple molecules; *Natl. Stand. Ref. Data Ser., Natl. Bur. Stand.* **1970**, *31*.
(78) Moore, C. E. Ionization potentials and ionization limits derived from the analysis of optical spectra. *Natl. Stand. Ref. Data Ser., Natl. Bur. Stand.* **1970**, 34.
(79) Huber, K. P.; Herzberg, G. *Molecular Spectra and Molecular Structure*; Van Nostrand: New York, 1979, Vol. *4*, p 170.
(80) Kooser, K.; Ha, D. T.; Granroth, S.; Itälä, E.; Partanen, L.; Nõmmiste, E.; Aksela, H.; Kukk, E. *J. Phys. B: At. Mol. Opt. Phys.* **2010**, *43*, 235103−1−10.
(81) Almeida, D. P.; Santos, A. C. F.; Homem, M. G. P.; Brito, A. N.; Souza, G. G. B. *J. Electron Spectrosc. Relat. Phenom.* **2007**, *155*, 109−112.
(82) Cavasso Filho, R. L.; Lago, A. F.; Homem, M. G. P.; Pilling, S.; Naves de Brito, A. *J. Electron Spectrosc. Relat. Phenom.* **2007**, *156−158*, 168−171.
(83) Suits, A. G.; Heimann, P.; Yang, X.; Evans, M.; Hsu, C. W.; Lu, K. T.; Lee, Y. T.; Kung, A. H. *Rev. Sci. Instrum.* **1995**, *66*, 4841−4844.
(84) Yates, B. W.; Hallin, E. L. *Rev. Sci. Instrum.* **2002**, *73*, 1602−1604.
(85) henke.lbl.gov/optical_constants/filter2.html.
(86) Samson, J. A. R.; Rayborn, G. H.; Pareek, P. N. *J. Chem. Phys.* **1982**, *76*, 393−397.
(87) Samson, J. A. R.; Masuoka, T.; Pareek, P. N.; Angel, G. C. *J. Chem. Phys.* **1987**, *86*, 6128−6127.
(88) Saito, N.; Suzuki, I. H. *Phys. Scr.* **1994**, *49*, 80−85.
(89) Holland, D. M. P.; Codling, K.; Marr, G. V.; West, J. B. *J. Phys. B: At. Mol. Opt. Phys.* **1979**, *12*, 2465−2484.